IEEE Photonics Journal
An IEEE Photonics Society Publication

Open Access

# Nonlinear Spectrum Compression of Negatively Chirped Picosecond Pulses in Dispersion-Shifted Telecom Fiber

Volume 12, Number 2, April 2020

Alexander Krylov
Andrey Senatorov
Yury Yatsenko

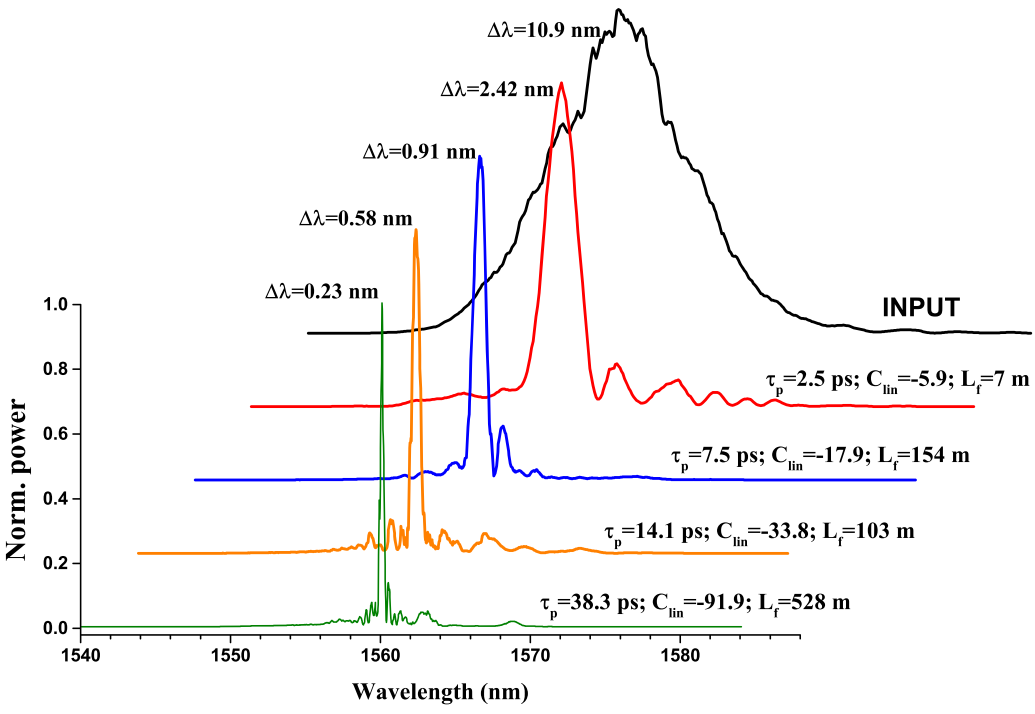


DOI: 10.1109/JPHOT.2020.2966301

# Nonlinear Spectrum Compression of Negatively Chirped Picosecond Pulses in Dispersion-Shifted Telecom Fiber

**Alexander Krylov, Andrey Senatorov, and Yury Yatsenko**

E. M. Dianov Fiber Optics Research Center of the Russian Academy of Sciences, 119333, Moscow, Russia

*DOI:10.1109/JPHOT.2020.2966301*
*This work is licensed under a Creative Commons Attribution 4.0 License. For more information, see http://creativecommons.org/licenses/by/4.0/*

Manuscript received November 19, 2019; revised December 30, 2019; accepted January 8, 2020. Date of publication January 12, 2020; date of current version March 9, 2020. This work was supported by Russian Science Foundation under Grant 19-12-00361. Corresponding author: Alexander Krylov (e-mail: krylov@fo.gpi.ru).

**Abstract:** We investigated both experimentally and numerically self-phase modulation-induced spectrum compression dynamics of negatively chirped picosecond Gaussian pulses in the low-loss dispersion-shifted telecom fiber near its zero dispersion wavelength (ZDW). It was experimentally observed linearly interpolated monotonous increase in spectrum compression ratio (SCR) with negative chirp growth of the incident pulse in the range from $-5.9$ to $-91.9$. According to numerical simulations, despite its small values in the vicinity of ZDW, fiber dispersion limits both SCR growth and spectrum compression quality expressed in terms of time-bandwidth product value and energy confinement ratio at larger chirp values ($|C| > 100$), in a combined action with self-phase modulation (SPM). Having optimized fiber length and pulse energy, we achieved record 49.2-fold spectrum compression of 38.3-ps, 2.08 nJ negatively chirped Gaussian pulses with compressed spectrum FWHM of 0.23 nm and $\approx$50% energy confinement at 1560 nm wavelength, leading to $\approx$13.3-times spectral brightness magnification. We believe that results obtained can be promising for ultra-short pulse laser systems development with enhanced spectral brightness.

**Index Terms:** Nonlinear spectrum compression, negatively chirped pulse, dispersion-shifted fiber, telecom fiber.

## 1. Introduction

Ultra-short pulse (USP) laser sources now become indispensable tools for various applications in science, medicine and industry [1], [2]. Recently, following tremendous developments in fiber optics technologies, USP laser sources on the basis of various rear-earth doped fibers emitting pico- and femtosecond pulses in different spectral bands have attracted much attention due to their efficiency, compactness, and environmental stability [3]–[6]. Meanwhile, apart from femtosecond fiber sources with wideband spectra (usually referred to as “optical combs”) being prospective for high-precision metrology [2]–[4], [7]–[10], transform-limited picosecond pulses with significantly reduced bandwidths are also beneficial for some applications requiring either spectral brightness or spectral resolution enhancement. These applications include, in particular, all-optical analog-to-digital converter development with increased bit resolution [11], various spectroscopic techniques [12], [13], quantum technologies [14] and others.

One possible approach to the problem of transform-limited narrow-bandwidth flexibly tunable pulse generation relies on a self-phase modulation (SPM) governed spectrum compression of seed femtosecond pulse (with hyperbolic secant or Gaussian envelopes) negatively pre-chirped either with external phase modulation [15] or in the dispersive element such as optical fiber [16], [17], prism [18], [19] or diffraction grating pair [20], [21] with simultaneous stretching up to picosecond durations, followed by their propagation through a fiber in the strongly nonlinear regime. This approach allows not only to take advantage of outstanding performance inherent to well-elaborated femtosecond fiber oscillators, but also to retrieve nearly transform-limited picosecond pulses with continuously tunable durations directly at the fiber out, which is quite beneficial in comparison with solid-state mode-locked USP sources (e.g., YAG family lasers) routinely generating narrowband picosecond pulses with fixed spectral widths. Besides, nonlinear spectrum compression technique is successfully employed for spectro-temporal imaging of femtosecond events [22], transform-limited pulse generation with rectangular-type spectrum [23], undistorted transmission of optical information through a telecommunication fiber link [24] and high-energy narrow-bandwidth picosecond pulse generation in powerful amplification systems [20], [21]. Thus, nonlinear spectrum compression can be utilized as an accompanying process that helps to improve a system performance. In view of this, the issue of coherent narrowband spectrum applications is much wider than simply a problem of transform-limited picosecond pulse generation that can be also realized in a mode-locked fiber laser [25] as well as with a narrow-bandwidth filter and the subsequent amplifier implementation.

During pulse propagation along a fiber, its negative chirp is gradually balanced by positive frequency modulation imposed by SPM, manifested as instantaneous frequency increase at the leading edge of the pulse and its reduction at the trailing edge [15]–[21], [23], [26], which is accompanied by energy redistribution from the wings to the center of the pulse spectrum, thus leading to its compression. Note that nonlinear spectrum compression is promoted in the case of appropriate pulse peak power adjustment in accordance with fiber length and its nonlinearity coefficient value [15]–[21], [23], [26]. However, nonlinear nature of SPM-induced frequency modulation accounts for broadband pedestal origination in the compressed spectrum, since the input linear chirp is only partially compensated for in the vicinity of the pulse center, whereas spectrum wings corresponding to pulse edges remain uncompressed. This prevents transform-limit condition achievement, noticeably deteriorating spectrum compression quality, expressed, in particular, as stagnation of spectral brightness enhancement [19]. In this regard, a number of ways including sinusoidal modulation of intra-pulse phase [27], optimal balancing of dispersion and nonlinearity impacts on pulse propagation by means of non-zero fiber dispersion implementation [23], [28], and parabolic pulse pre-shaping [15], [17] has been proposed in order to correct SPM-induced nonlinear distortions of a pulse chirp, thus reaching its better compensation across the whole pulse envelope. The latter seems to be highly attractive for spectrum compression (SC) quality improvement, since SPM-induced frequency modulation is purely linear only for a pulse with an ideally parabolic temporal intensity profile (and parabolic spectrum shape as well), which remains unchanged within pulse propagation throughout a fiber [15], [17].

Recently it has been reported on 12.2-fold nonlinear spectrum compression to within 12% of Fourier transform limit with more than 64% energy confinement ratio (the energy fraction in a compressed spectral peak) after propagation through 1-km-long highly nonlinear fiber with small positive dispersion ($\beta_2 = +0.96$ ps$^2$/km) of 70 ps, 0.1 nJ negatively-chirped parabolic pulses at 1552.5 nm wavelength, which were formed using a complex pulse shaper consisting of elements with angular dispersion and liquid-crystal matrix-based amplitude and phase spatial beam modulator [17]. This work should also be highlighted as demonstrating record SC ratio with nearly transform-limited picosecond pulses, obtained so far using the nonlinear spectrum compression technique in the telecom spectral band.

Though nonlinear spectrum compression has been already realized in various spectral bands using Ti:sapphire [18], [19], [23], [26], Yb- [15], [16], [20], [21], Er- [17], [24], [29] and Tm- [30] USP sources, there is a lack of systematic experimental studies on crucial SC parameters (spectrum compression ratio, time-bandwidth product and energy confinement ratio) evolution with input

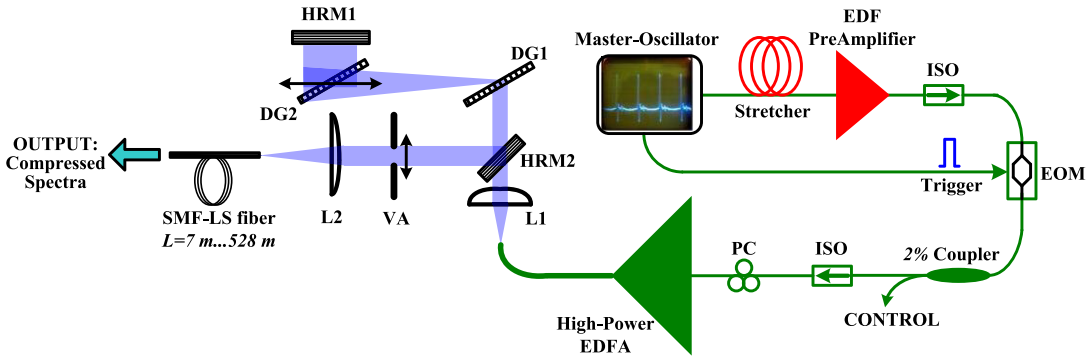


Fig. 1. Experimental setup for nonlinear spectrum compression study. (ISO – in-line fiber isolator; PC-polarization controller; fibers with positive and negative GVD are red- and green-colored respectively).

pulse-width (and negative chirp) tuning, especially in the telecom band. As well, practical limits of spectral brightness enhancement offered by the nonlinear SC technique have not been fully clarified yet.

In this work we carefully investigate both experimentally and numerically self-phase modulation-induced spectrum compression dynamics of negatively chirped picosecond Gaussian pulses in the low-loss dispersion-shifted telecom fiber near its zero dispersion wavelength. It was experimentally observed linearly interpolated monotonous increase in spectrum compression ratio (SCR) with negative chirp growth of the incident pulse in the range from $-5.9$ to $-91.9$. However, according to numerical simulations, it has been found that fiber dispersion accounts for a limitation of both SCR growth and compression quality, expressed in terms of time-bandwidth product value and energy confinement ratio at larger chirp values ($>100$), owing to self-phase modulation-governed complex propagation dynamics of highly-chirped pulses in the vicinity of ZDW. By fiber length and pulse energy optimization, we achieved record 49.2-fold spectrum compression of 38.3-ps, 2.08 nJ negatively-chirped Gaussian pulses with compressed spectrum FWHM of 0.23 nm and $\approx$50% energy confinement ratio at 1560 nm wavelength, corresponding to $\approx$13.3-fold spectral brightness magnification.

## 2. Experimental Details

The experimental setup for nonlinear spectrum compression study is sketched in Fig. 1. It consists of two main blocks that account for generation of negatively chirped pulses with flexibly tunable durations [31]: (i) home-built high-energy erbium all-fiber USP source emitting chirped Gaussian pulses at $\approx$1560 nm wavelength and (ii) adjustable dispersion delay line (DDL) based on a diffraction gratings' pair to steer output pulse-width, simultaneously imposing certain amount of negative linear chirp.

The erbium all-fiber USP source was built according to well-known Master-Oscillator Chirped Pulse Amplification (MOCPA) concept. Positively-chirped Gaussian-type pulses from the home-made hybridly mode-locked Er-doped fiber (EDF) master-oscillator (38.1 MHz repetition rate, 9 mW average power, $\approx$1560 nm generation wavelength) [32] were stretched up to $\approx$70 ps width (acquiring positive chirp) in the 31-m-long germanium-silicate fiber (30 mol.% $GeO_2$ in the 2.2-$\mu$m core) with enhanced positive group velocity dispersion (GVD) of $\beta_2 = +99.8$ ps$^2$/km, then pre-amplified in the 5-m-long core-pumped EDF up to 109 mW average power and decimated by means of the pigtailed EOM (JDSUniphase) with 3.6 dB loss figure, giving rise to 15-fold repetition rate reduction (down to 2.54 MHz) at $\approx$20 dB decimation contrast. Having passed through the isolator and auxiliary coupler with 2% control port, chirped pulses entered high-power amplifier (EDFA) built from 4-m-long Er-doped LMA double-clad fiber with $\approx$35 $\mu$m core diameter and $\approx$15 nm gain

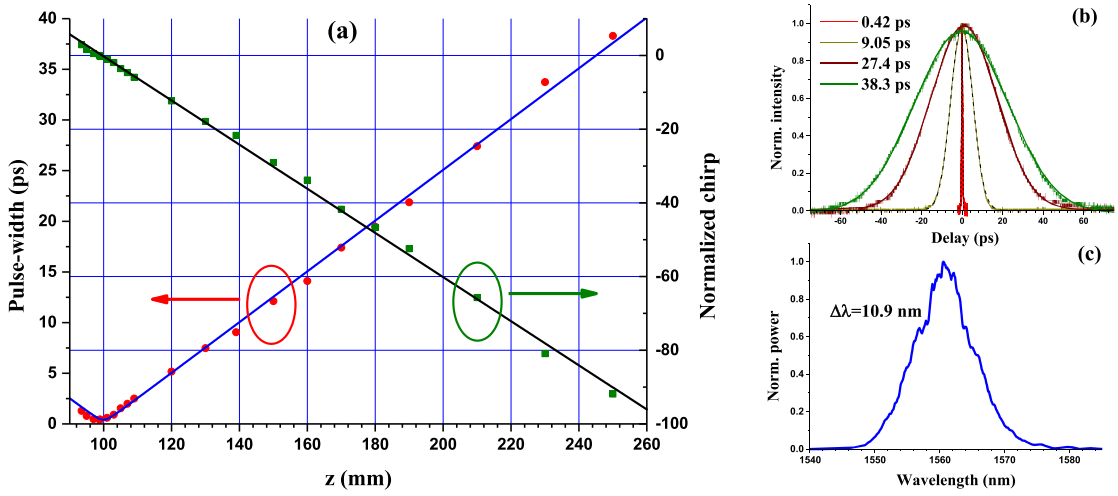


Fig. 2. (a) Pulse-width (left axis) and normalized chirp (right axis) dependence on a distance (z) between gratings. (b) ACTs and (c) spectrum of negatively-chirped Gaussian pulses after DDL at 50 mW average power.

bandwidth [33], pumped with 30 W multimode laser diode at 980 nm wavelength belonging to the $^4\mathbf{I}_{15/2}\rightarrow{}^4\mathbf{I}_{11/2}$ absorption band of $Er^{3+}$ ions in silica glass matrix.

As a result, pulses from the erbium all-fiber CPA source were positively-chirped with durations slightly varying from $\tau_p = 23.2$ ps to 25.2 ps (according to Gaussian fit) within output pulse energy growth from 14 nJ to 759 nJ – the maximal value corresponding to ≈2 W output average power. Meanwhile, as it was measured using integrating photo-detector, decimated pulse after amplification confined major portion (≈95%) of total energy [31]. However, in view of limited gain bandwidth of high-power EDFA, pulse spectrum width (at half maximum) does not exceed ≈12 nm over the whole range of output pulse energies, with the center wavelength slightly tuning around ≈1560 nm.

Radiation from the erbium USP source output was collimated with 20-mm focus plano-convex lens L1 and launched into the adjustable double-pass DDL composed of a pair of highly efficient polarization-independent transmission diffraction gratings DG (Ibsen Photonics) with 940 l/mm density (diffraction efficiency was more than 93% at 1560 nm wavelength) and two highly-reflective silver mirrors HRM1 and HRM2, the latter being used to pick the beam out. DDL introduced ≈1 dB attenuation regardless of polarization state of incident light, while output beam exhibited small ellipticity of about 10%. In order to adjust gratings' separation, DG2 was mounted on a translation stage with 10 $\mu$m resolution screw, which enabled pulse-width and chirp variation in controllable manner.

Within experiments average power at the DDL out was tuned between 30 mW and 110 mW with corresponding pulse energy ranged from 11.2 nJ to 41.2 nJ, which, nonetheless, ensured operation of high-power amplification stage in a linear mode with negligible deviations in output spectrum width and pulse duration.

The dependence of a Gaussian pulse-length at half-maximum ($\tau_p$) measured at 50 mW average power (19 nJ pulse energy) after DDL on a distance (z) between gratings is plotted on Fig. 2a. Herewith, the evolution of normalized linear pulse chirp ($C_{lin} = (\partial^2\varphi/\partial t^2)\cdot\tau_p{}^2/4\ln 2$ evaluated at $t = 0$ in retarded frame corresponding to a Gaussian pulse center) is demonstrated as well, which is calculated using measured pulse-widths $\tau_p$ as $|C_{lin}| = ((\tau_p/\tau_{min})^2-1)^{0.5}$, where $\tau_{min} = 417$ fs is shortest pulse duration observed at $z_{min} \approx 99$ mm. As seen on Fig. 2a, $\tau_p(z)$ plot is well fitted with the function $\tau_p(z) = \tau_{min}(1+((z-z_0)/L_D)^2)^{0.5}$ responsible for group velocity dispersion (GVD)-governed evolution of Gaussian pulse-width in a linear dispersive media with appropriate

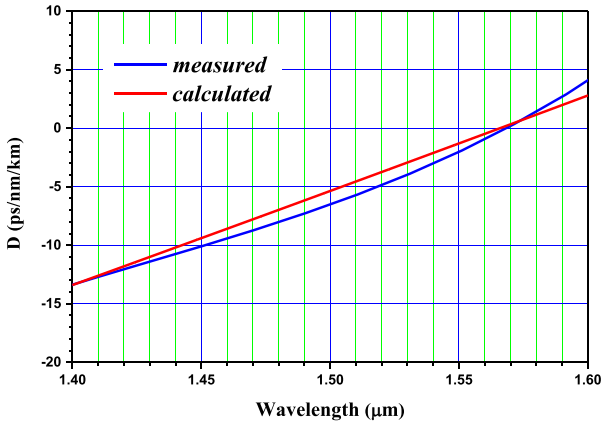


Fig. 3. GVD of the SMF-LS fiber.

dispersion length $L_D = (1/4\ln 2)\cdot\tau^2_{min}/|\beta_2| = 1.663 \pm 0.017$ mm and focus position (the point of a shortest pulse-width) $z_0 = 99.94 \pm 0.68$ mm. Moreover, as it is expected for Gaussian pulse, normalized chirp evolution $C_{lin}(z)$ is accurately interpolated by linear function $C_{lin}(z) = -(z-z_0)/L_D$ with the same $L_D$ and $z_0$ values. As a matter of fact, linear chirp inverts its sign in the focus point $z_0$ (at which $C_{lin} = 0$), yielding negatively-chirped pulses at the DDL out with more than ≈100 mm gratings' separation.

A number of intensity autocorrelation traces (ACT) for negatively-chirped pulses measured with FEMTOCHROME non-collinear autocorrelator are presented in Fig. 2b, whereas typical pulse spectrum registered with ANDO spectrum analyzer at 50 mW average power after DDL is shown in Fig. 2c. In contrast to ACTs, well-fitted with proper Gaussian functions, pulse spectrum exhibits visible distortions, which we attribute mostly to both amplitude and phase aberrations translated from the master-oscillator with rather complex spectrum shape [32], in conjunction with regular amplitude modulation exerted by EOM within pulse decimation process, further gained in high-power EDFA [31]. Since amplitude distortions of a pulse spectrum are routinely accompanied by appropriate nonlinear phase aberrations to match its Gaussian temporal profile, pulses leaving erbium USP source accumulate excessive nonlinear chirp $C_{nl}$ that can hardly be compensated by DDL with Fourier limit achieving, which, in particular, results in time-bandwidth product rising up to $TBP_{min} \approx 0.6$ even for the shortest pulse-width of $\tau_{min} = 417$ fs. Note that in order to reduce an influence of stochastic birefringence and third-order dispersion (TOD) in highly-nonlinear stretching fiber responsible for pulse envelope distortions, its length together with input polarization state was carefully adjusted.

As mentioned above, peak power is a crucial parameter governing nonlinear spectrum compression dynamics during negatively chirped pulse propagation along a fiber. Therefore, collimated beam from the DDL out went through a power attenuator on the basis of a variable slit with 10 $\mu$m resolution for precise control of energy and, as a result, peak power of negatively chirped pulses further launched to the fiber. It is worth to emphasize that a variable attenuator (VA) is a key element in the scheme of nonlinear spectrum compression that accounts for compressed spectra optimization at given fiber length and input negative chirp value.

Having passed through the variable attenuator, negatively-chirped pulses were then coupled into the low-loss dispersion-shifted telecom SMF-LS fiber (LEAF Submarine, @CORNING, USA) using 18-mm focus aspheric lens L2. The fiber introduces small optical losses of less than 0.25 dB/km according to the product datasheet. Spectral dependence of fiber GVD shown in Fig. 3 (red curve) was calculated using COMSOL software on the basis of measured refractive index profile. Besides, we measured SMF-LS second-order dispersion by means of a low-coherence interferometric technique [34] (blue curve in Fig. 3) to reveal rather good agreement with calculated one. Thus,

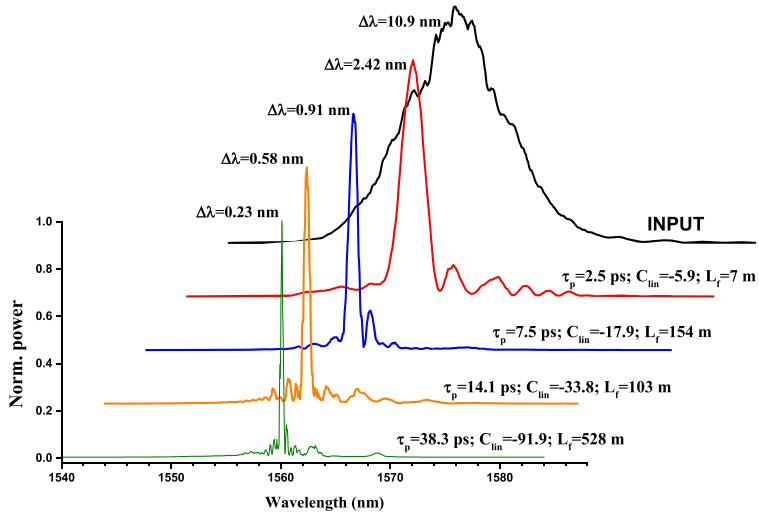


Fig. 4. Compressed spectra for different negative chirp values together with input one (black).

SMF-LS fiber introduces small positive GVD of $\beta_2 \approx +0.628$ ps$^2$/km at the pulse center wavelength $\lambda_c \approx 1560$ nm being slightly blue-shifted with respect to the fiber ZDW of $\lambda_{zd} \approx 1566$ nm. Taking into account nonlinear refractive index of $n_2 = 2.6{\cdot}10{-}16$ cm$^2$/W and effective cross-section area of $A_{eff} = 52$ $\mu$m$^2$ (matching with $\approx$8.1 $\mu$m mode-field diameter), fiber nonlinearity coefficient was estimated to be $\gamma = 2.01$ (W·km)$^{-1}$ at 1560 nm wavelength.

Within experiments SMF-LS fiber length was varied from 7 m to 528 m depending on the negatively chirped pulse-width tuned between 2.5 ps and 38.3 ps (with corresponding linear chirp ranged from $C_{lin} = -5.9$ to $-91.9$), while input pulse energy was optimized in order to improve both spectrum compression ratio and compression quality (expressed in terms of energy confinement ratio) for given fiber length and negative chirp value.

## 3. Experimental Results

A set of compressed spectra for different input pulse-widths (and negative chirp values) that have been optimized according to the procedure described in Sec. 2, together with input one are illustrated in Fig. 4. Note that SMF-LS fiber length $L_f$ and normalized chirp value $C_{lin}$ are pointed out along with pulse duration for each spectrum in Fig. 4. Meanwhile, compressed peaks were fitted with suitable Gaussian functions to retrieve their 3-dB widths ($\Delta\lambda$) and further calculate energy confinement ratio ($\eta$) and time-bandwidth product (TBP) values.

As a matter of fact, each spectrum from Fig. 4 accommodates noticeably modulated uncompressed pedestal responsible for degradation of both energy confinement ratio and peak-to-pedestal contrast, which is a physical manifestation of nonlinear nature of SPM-induced frequency modulation that balances negative linear chirp only in the vicinity of the Gaussian pulse center [15]–[21], [23], [26]. As a result, peak-to-pedestal contrast and energy confinement ratio do not exceed 11.2 dB and 77%, respectively, for all compressed spectra recorded.

The outcome experimental data on spectrum compression ratio ($K_S$) and energy confinement ratio ($\eta$) evolutions with pulse stretching ratio ($K_P = \tau_p/\tau_{min}$) increase are plotted on Fig. 5a. While the former dependence ($K_S(K_P)$) quite well approximated by linear function with a positive slope $dK_S/dK_P = 0.528{\pm}0.022$ demonstrates monotonous growth, the latter ($\eta(K_P)$) evidently goes down, which is a characteristic feature of SPM-induced spectrum compression. Moreover, for compressed spectra to be improved, SMF-LS fiber was significantly elongated (from 7 m to 528 m) with negatively chirped pulse-width tuning between 2.5 ps and 38.3 ps (corresponding fiber length is given in brackets near each data point in Fig. 5a).

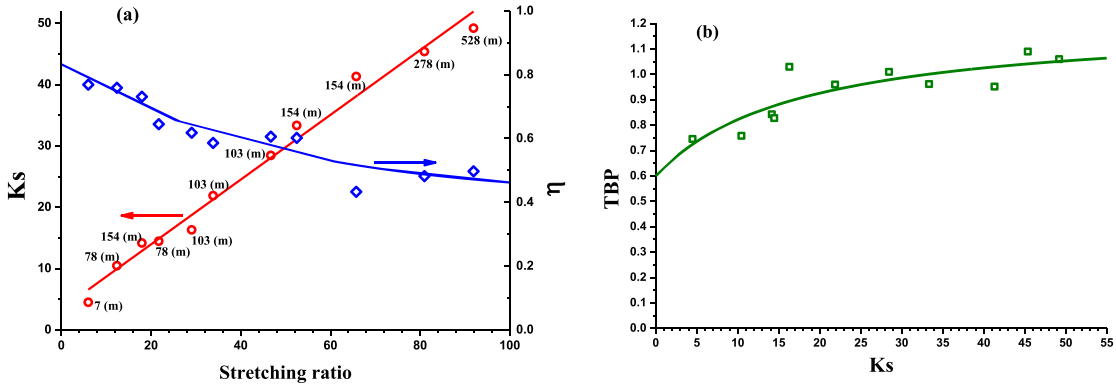


Fig. 5. (a) Spectrum compression ratio (left axis) and energy confinement ratio (right axis) evolutions with pulse stretching ratio $K_P$. (b) TBP versus spectrum compression ratio $K_S$.

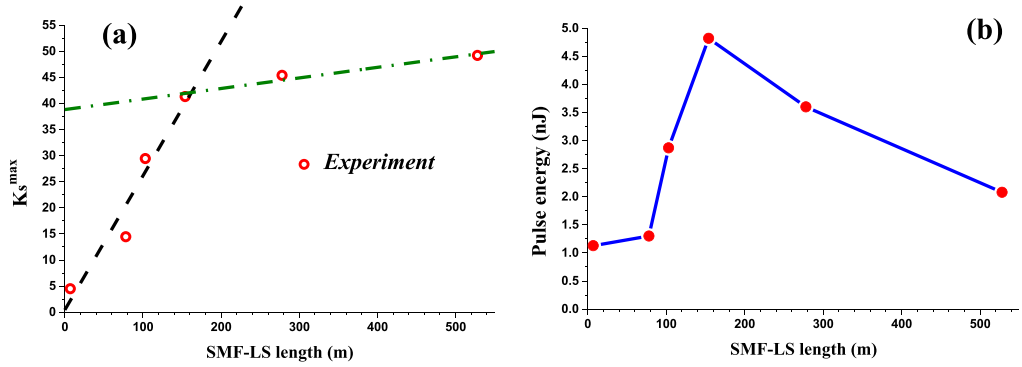


Fig. 6. (a) Maximum SCR ($K_S^{max}$) and (b) corresponding input pulse energy dependence on the SMF-LS fiber length.

As it is expected in the case of such a low GVD value, used fiber pieces are significantly shorter than dispersion length $L_D$ and even dechirping length $L_C = L_D \cdot C_{lin}/(C^2_{lin}+1)$ for input pulses, which means insignificant role of second-order dispersion during SPM-dominant pulse propagation along a fiber, thus leading to minor variations in its duration. In view of this, we calculate time-bandwidth product using measured spectrum FWHM and input pulse-width to attain TBP dependence on spectrum compression ratio depicted in Fig. 5b, which demonstrates saturated growth affirmed by a careful fitting with a proper rational function (TBP $\propto K_P/K_S$) with a saturated $TBP^{sat} = 1.21 \pm 0.06$. Moreover, it can be simply determined using certain fitting parameters that for hypothetical $K_S = 1$ we obtain TBP = 0.63, being quite close to that of the shortest pulse after DDL, which, thus makes further evidence in favor of approximation model adequacy.

Further we studied experimental dependences of maximum SCR ($K_S^{max}$) and appropriate pulse energy ($E_p^{opt}$) on SMF-LS fiber length (Fig. 6a and b), in order to find out requirements imposed on pulse parameters and fiber length from the point of prospects of further SCR enhancement. Herewith, $K_S^{max}(L_f)$ plot consists of two distinct stages separated by the edge point $L_f = 154$ m, individually fitted by proper linear functions with strictly different positive slopes of $(dK_S^{max}/dL_f)_1 = 0.26 \pm 0.05$ m$^{-1}$ and $(dK_S^{max}/dL_f)_2 = (0.20 \pm 0.04) \cdot 10^{-1}$ m$^{-1}$. Meanwhile, as seen in Fig. 6b, optimal pulse energy monotonically grows, maintaining peak power close to ≈150 W (except for the first point $L_f = 7$ m, for which $P_{peak} = 452$ W), until reaching maximum value of 4.8 nJ at the same edge point of $L_f = 154$ m, followed by its gradual reduction with further fiber elongation, also

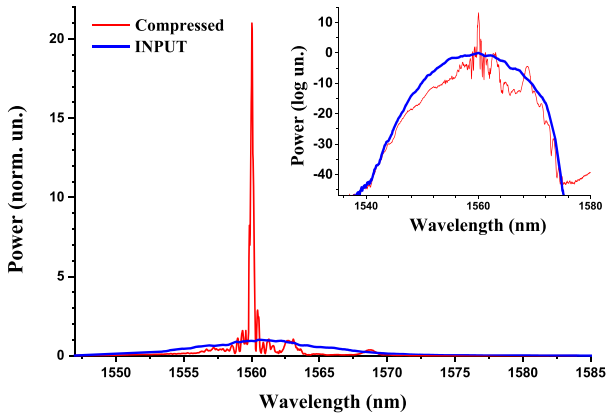


Fig. 7. Compressed spectrum in the case of highest SCR together with input one normalized to the same pulse energy in linear and logarithmic (the Inset) scales.

accompanied by peak power diminishing to the minimal value of $P_{peak}^{min} = 50.3$ W at $L_f = 528$ m. Thus, according to experimental results, significant SMF-LS fiber elongation together with peak power reduction is expected to achieve SCR increase with onward growth of negative pulse chirp.

Compressed spectrum with $\Delta\lambda_{FWHM} = 0.23$ nm, $\eta \approx 50\%$ and TBP $= 1.06$ corresponding to the highest SCR ($K_S = 49.2$) obtained for 38.3 ps pulse with 2.08 nJ energy and $L_f = 528$ m, together with input one, normalized to the same pulse energy, are presented in Fig. 7 in order to emphasize significant spectral brightness enhancement ($K_B \approx 13.3$) achieved using nonlinear SC of negatively chirped picosecond Gaussian pulses.

## 4. Numerical Simulation

We have numerically simulated nonlinear spectrum compression of negatively chirped picosecond pulses using generalized Schrödinger equation for complex slowly varying pulse amplitude in spectral domain, which takes into account Kerr nonlinearity, higher-order fiber dispersion terms and Raman response [35]. At the moment we are not aware of nonlinear chirp distribution across the pulse, which prevents complete pulse characterization, needed for explicit reproduction of experimental conditions. Therefore, to study the dynamics of spectrum compression during pulse propagation along a fiber, purely linear chirped Gaussian pulses with parameters close to experimentally measured values were employed.

Spectrum compression dynamics, calculated for Gaussian pulse with 10.6 nm spectrum FWHM, 452 W peak power ($E_p = 1.13$ nJ) and negative chirp $C_{lin} = -5.9$ (the lowest one) is demonstrated in Fig. 8.

As shown in Fig. 8c, spectrum compression ratio growth during linear compression stage ($\varphi_{SPM} < \pi$) is gradually saturated after propagation through 3-m-long fiber segment, further reaching its maximum value ($K_S = 4.4$) at $L_f = 9.1$ m. The strongly nonlinear behavior of spectrum compression process in the fiber segment from $L_f = 3$ m to 9 m is manifested as symmetrically located side-lobes appearance in the pulse spectrum as shown in Fig. 8a, b, as well as complex behavior of energy confinement ratio having local maximum of $\eta = 0.85$ at $L_f = 5.5$ m, followed by its rapid reduction to $\eta = 0.5$ at the point of maximum compression ($L_f = 9.1$ m), due to the growth of lateral satellites (Fig. 8b and d). It is worth to note that SC parameters calculated for $L_f = 7$ m ($K_S = 4.1$, $\eta = 0.8$, TBP $= 0.6$) are in good agreement with experimental ones ($K_S^{exp} = 4.5$, $\eta^{exp} = 0.77$, $TBP^{exp} = 0.75$), which thus makes evidence of insignificant impact of nonlinear pulse chirp $C_{nl}$ on spectrum compression dynamics in the case of low negative chirp values.

As it follows from Fig. 9a, for input Gaussian pulse with the highest negative chirp of $C_{lin} = -91.89$ realized in the experiment, and other parameters equal to experimental ones

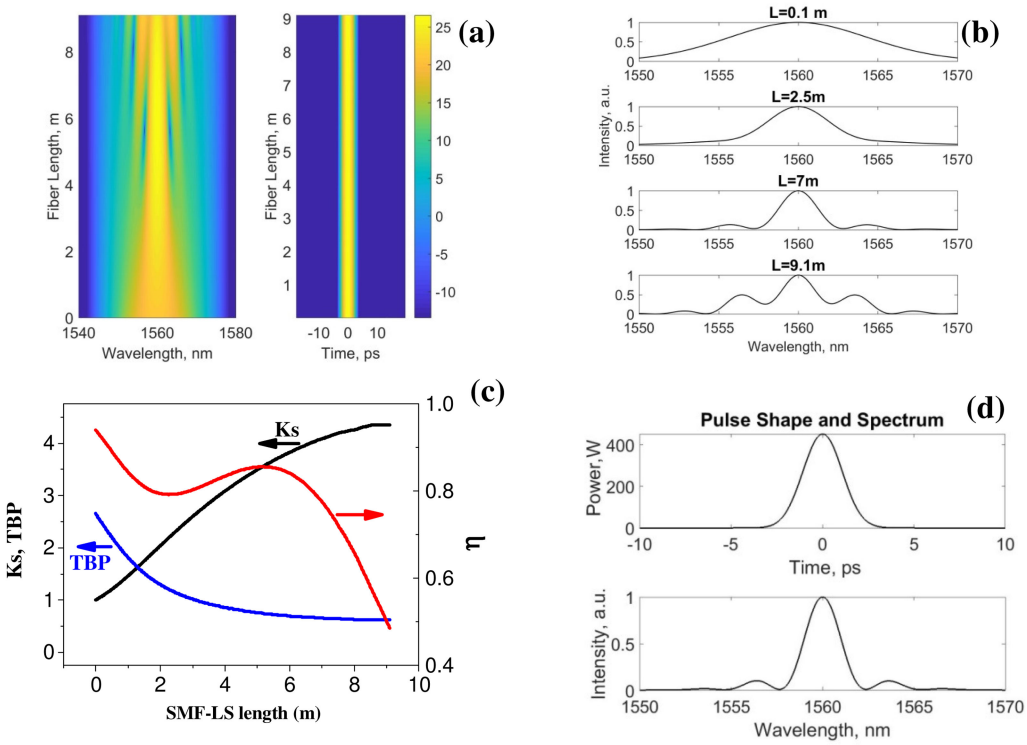


Fig. 8. Evolution of the spectral and temporal characteristics of the Gaussian input pulse with the negative chirp $C_{\rm lin} = -5.9$ during its propagation along SMF-LS fiber. (a) Densitogram of the spectrum and pulse envelope evolutions. (b) Pulse spectrum at different fiber lengths. (c) Spectrum compression ratio ($K_S$), time-bandwidth product (TBP) and energy confinement ratio ($\eta$) dependence on the SMF-LS fiber length. (d) Pulse envelope and spectrum at $L_f = 7$ m.

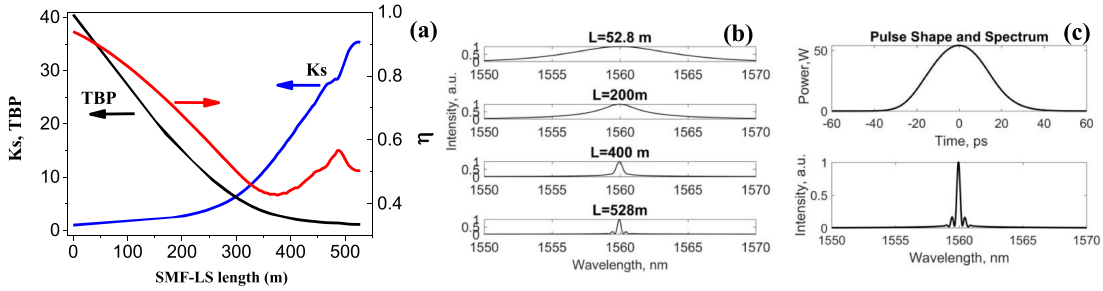


Fig. 9. Evolution of the spectral and temporal characteristics of the Gaussian input pulse with the negative chirp of $C_{\rm lin} = -92$ during its propagation along SMF-LS fiber. (a) Spectrum compression ratio ($K_S$), time-bandwidth product (TBP) and energy confinement ratio ($\eta$) dependence on the SMF-LS fiber length. (b) Pulse spectrum at different fiber lengths. (c) Pulse envelope and spectrum at $L_f = 528$ m.

($\Delta\lambda = 10.6$ nm, $P_{\rm peak} = 50.3$ W, $E_p = 2.08$ nJ), optimal fiber length for maximum spectrum compression is obtained to be $L_f^{opt} = 528$ m, which is coincident with the fiber length used in the experiment. However, calculated SCR of $K_S^{calc} = 35.1$ turned out to be noticeably less than experimentally observed value ($K_S^{\rm exp} = 49.2$). We ascribe this discrepancy to the different contributions from the nonlinear part of the pulse chirp to the SPM-induced spectrum compression for highly-chirped Gaussian and real pulses resulting in different partial compensation for a nonlinear phase imposed by SPM.

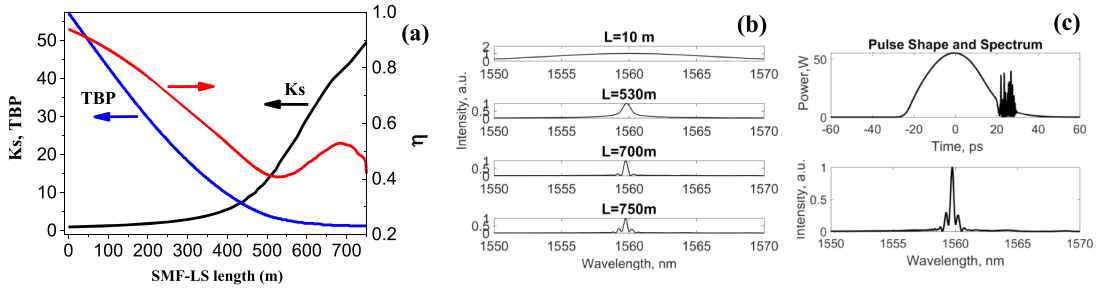


Fig. 10. Evolution of the spectral and temporal characteristics of the Gaussian input pulse with the negative chirp $C_{lin} = -130$ and a peak power of 54.3 W during its propagation along SMF-LS fiber. (a) Spectrum compression ratio ($K_S$), time-bandwidth product (TBP) and energy confinement ratio ($\eta$) dependence on the SMF-LS fiber length. (b) Pulse spectrum at different fiber lengths. (c) Pulse envelope and spectrum at $L_f = 750$ m.

Despite the large chirp value, spectrum compression dynamics is similar to that one occurred in the case of lowest negative chirp depicted in Fig. 8c, with a local maximum of energy confinement ratio ($\eta \approx 0.57$) at $L_f = 487$ m and $K_S = 28.6$. The pulse spectrum at the point of maximum compression ($L_f = 528$ m) consists of the central maximum and symmetrically located well-pronounced side-peaks with equal amplitudes, as seen in Fig. 9b and c. Meanwhile, as it is also confirmed by the experiment, SC quality is noticeably reduced in this case (TBP = 1.14, $\eta = 0.51$).

From the calculations it follows that in order to obtain $K_S$ values comparable to experimental ones, chirp value $C_{lin}$ should be further increased. Herewith, to reduce an optimal fiber length, while maintaining the magnitude of compression ratio $K_S$, it is necessary to enlarge the input pulse peak power. Thus, for a Gaussian pulse with 2.08 nJ energy ($P_{peak} = 54.3$ W) and a linear chirp value of $C_{lin} = -130$, the spectrum compression ratio reaches $K_S = 49.6$ at the optimal fiber length of $L_f^{opt} = 750$ m as seen in Fig. 10a.

A distinct feature of the SC process at $C_{lin} = -130$ is the origination of a modulation structure at the trailing edge of the pulse, which is accompanied by the asymmetric modulation background together with unequal side-lobes amplitudes in the spectral domain (Fig. 10c). Since long-wavelength components of the negatively chirped pulse spectrum, located at the trailing edge of the pulse envelope, fall into the region of negative fiber dispersion, modulation instability-induced pulse envelope breakdown occurs, leading to the formation of a pronounced modulation structure. Nonetheless, such a modulation structure does not prevent SC realization with suitable quality ($\eta = 0.4$ and TBP = 1.15) that is not much worse than that for $C_{lin} = -92$, considered above.

In order to evaluate modulation instability influence within spectrum compression process in more details, we numerically studied the evolution of spectral and temporal pulse characteristics at optimal fiber lengths ($L_f^{opt}$) corresponding to the maximum $K_S$ values with input peak power growth at the constant input chirp $C_{lin} = -130$ and pulse duration $\tau_p$=32.3 ps (Fig. 11).

Figure 11a shows the dependence of spectrum compression ratio and corresponding optimal fiber length ($L_f^{opt}$) on the input peak power in the range from 10 W to 3 kW. Here we can distinguish three areas of peak power with strictly different SC quality observed. In the middle area of moderate peak powers from 50 W to 1000 W ($L_f^{opt}$ varies in this case from 750 m to 41 m), the SC ratio is kept close to $K_S \approx 50$ with minor deviations, while SC quality is comparable to that one shown in Fig. 10. Outside this area, SC quality noticeably deteriorates, with strictly different distortions of spectral and temporal pulse characteristics observed for higher and lower peak powers. Typical pulse envelope and spectrum for higher peak power range ($P_{peak} > 1000$ W) at the point of maximum spectrum compression ($L_f = 27$ m, $K_S = 44$) are shown in Fig. 11b for the peak power of $P_{peak} = 1500$ W. Here a significant growth of modulation amplitude at the pulse trailing edge is evidently seen, which is associated with modulation instability gain increase at higher peak powers ($g_{max} = 2\gamma P_{peak}$) also leading to heavily asymmetric spectrum shape.

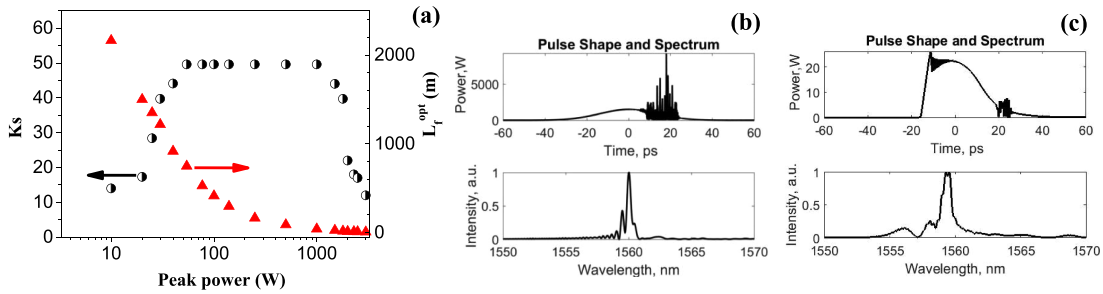


Fig. 11. (a) Dependence of the spectrum compression ratio ($K_S$), and optimal fiber length ($L_f^{opt}$) corresponding to the maximum compression on the peak power for input Gaussian pulse with $C_{lin} = -130$. (b) Pulse envelope and spectrum at the maximum compression point for a pulse peak power of $P_{peak} = 1500$ W ($L_f^{opt} = 27$ m). (c) Pulse envelope and spectrum at the maximum compression point for a pulse peak power of $P_{peak} = 20$ W ($L_f^{opt} = 1500$ m).

Pulse envelope and spectrum at $P_{peak} = 20$ W (lower peak power range) at the point of maximum spectrum compression ($L_f = 1500$ m, $K_S = 17.3$) are displayed in Fig. 11c. In contrast to previous case of higher peak power, positive fiber dispersion makes a significant contribution to the temporal distortions of a pulse, expressed as a steepening of the pulse leading edge owing to dispersion-assisted slowdown of the short-wavelength spectral components. Thus, in co-action with SPM, a complex modulation structure of the pulse spectrum is formed, which prevents further compression. It should be noted that fiber dispersion significantly affects SC dynamics at relatively low values of $L_f$ compared to $L_D$ ($L_f/L_D = 1.5{\cdot}10^{-2}$).

## 5. Discussion

As it follows from experimental data, displayed in Fig. 5, nearly linear monotonous growth of spectrum compression ratio from $K_S = 4.5$ to 49.2 has been observed within pulse-width tuning between 2.5 ps and 38.3 ps (corresponded to linear chirp ranged from $C_{lin} = -5.9$ to $-91.9$). Herewith, energy confinement ratio goes down from $\eta = 77\%$ to $\approx$50%, while TBP value rises from 0.76 to 1.06, the latter exhibiting saturation behavior.

It is noteworthy that such a record spectrum compression ratio was achieved mainly as a result of both SMF-LS fiber length optimization and careful pulse energy (and, of course peak power) adjustment. Indeed, an application of “two degrees of freedom” is strictly beneficial if compared to other experimental studies either employing fiber pieces with definite lengths [16], [17], [20], [21], [26], [30] or suffering from a lack of peak power [18], [19] and limited chirp values [15]. Moreover, it is fairly evident that an implementation of high-end low-loss dispersion-shifted telecom fiber with uniformly distributed dispersion and nonlinearity along its length promotes SC quality improvement, since longer fiber segments can be easily applied. Besides, fibers with low positive GVD are more suitable for higher SCR realization [17], [19], which also allows to avoid undesirable effects associated with solitonic propagation such as modulation instability and dispersive waves emission for negative chirp values up to $C_{lin} = -100$, as confirmed by numerical consideration in Sec. 4.

In order to elucidate prospects of spectral brightness enhancement with SCR increase, we study Strehl ratio (S) dependence on pulse stretching ratio ($K_P$) shown in Fig. 12 (Strehl ratio expressed as $S = \eta{\cdot}(TBP_{min}/TBP)$, determines compressed spectrum quality in terms of spectral brightness [17], [27], [28], [36]). Its obvious saturation trend with $S^{sat} = 0.25{\pm}0.05$ favors SCR rising without stagnation of brightness increase ratio ($K_B = K_S{\cdot}S$), provided that nearly linear SCR evolution with negative chirp growth according to Fig. 5a is preserved.

It is also interesting to compare SC quality achieved at the same (or at least close) SCR values to that one reported in previously emphasized work [17] with parabolic negatively chirped pulses

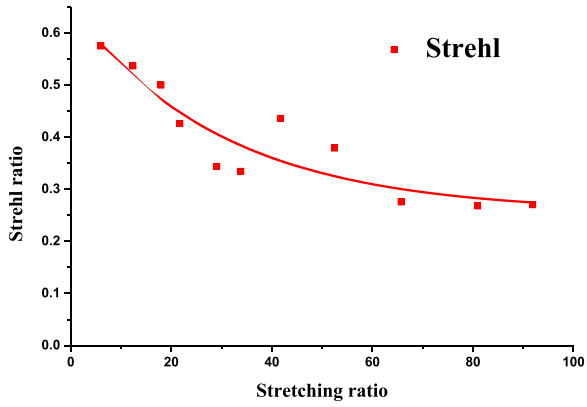


Fig. 12. Strehl ratio evolution with negatively-chirped pulse-width growth.

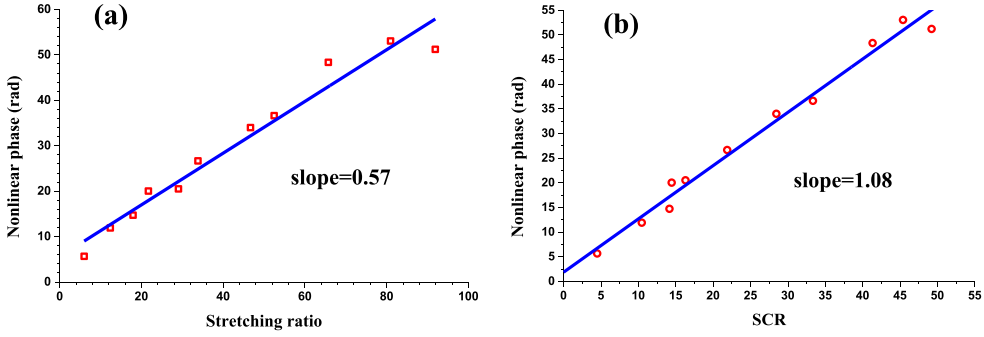


Fig. 13. SPM-induced phase shift versus stretching ratio $K_P$ (a) and spectrum compression ratio $K_S$ (b).

employed. Hereby, at $K_S \approx 11$ ($\tau_p = 5.2$ ps, $E_p = 0.44$ nJ, $L_f = 78$ m) Strehl ratio and time-bandwidth product amount to $S = 0.54$ and $TBP = 0.758$ respectively, being quite close to the same values from [17] ($S = 0.57$, $TBP = 0.745$) at the highest $K_S = 12.2$, which we attribute to the application of "two degrees of freedom" option to SC optimization procedure.

Although negative pulse chirp cannot be compensated by the nonlinear frequency modulation imposed by SPM for all intra-pulse times t at any propagation distance $L_f$ along a fiber, the instantaneous intra-pulse frequency $\delta\nu(L_f,t)$ linearized via its expansion in a Taylor's series around a Gaussian pulse center (the maximum peak power point) can be zeroed for all t if the following condition is fulfilled: $\varphi_{SPM}^{max} = (1/2)K_P(*)$, where $\varphi_{SPM}^{max} = L_f/L_{NL} = L_f \cdot \gamma \cdot P_{peak}$ is a maximum SPM-induced phase shift acquired by a Gaussian pulse after propagation distance $L_f$ [27], [28]. This expression can be rewritten with some approximation in terms of negative pulse chirp as $C_{lin} \approx -2 \cdot \varphi_{SPM}^{max}$ $(**)$, which is, however valid with better accuracy for $|C_{lin}|>>1$. Note that expression $(**)$ implies an existence of distinct $\varphi_{SPM}^{max}$ in the case of optimal $C_{lin}$ compensation, being independent of fiber parameters and pulse peak power.

Hence, to make insight into the relation between SPM-induced phase shift $\varphi_{SPM}^{max}$ and pulse stretching ratio $K_P$ for optimized experimental conditions, we plot $\varphi_{SPM}^{max}(K_P)$ dependence shown in Fig. 13a. The data are accurately fitted by a linear function with the slope $d\varphi_{SPM}^{max}/dK_P = 0.57 \pm 0.04$ being quite close to the theoretical coefficient (1/2) in eq.$(*)$, which makes evidence of negative pulse chirp balancing by linearized SPM-induced frequency modulation (especially for $\varphi_{SPM}^{max} \gg 1$) across the pulse, that is necessary condition for optimized SC achievement.

In order to corroborate the existence of certain SPM-induced phase shift $\varphi_{SPM}^{max}$ adherent to optimized SC for given negative chirp value, we realized nonlinear spectrum compression of

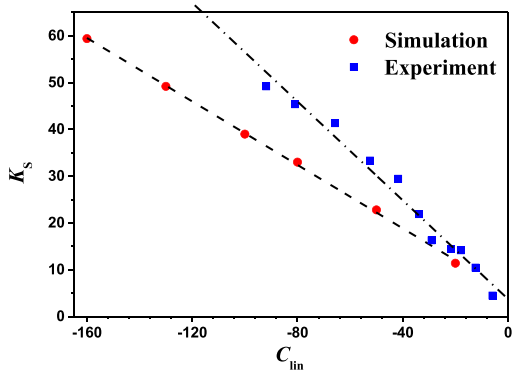


Fig. 14. Dependence of the maximum spectrum compression ratio ($K_S$) on the negative pulse chirp ($C_{lin}$) for a Gaussian pulse with the input peak power of 100 W and a fixed spectrum width of 11 nm (circles) together with experimental data (squares).

7.5-ps-long negatively chirped pulses ($C_{lin} = -17.9$) using two SMF-LS fiber pieces, one of them ($L_f^1 = 154$ m) being twice longer than the other ($L_f^2 = 78$ m). Having optimized SC in both cases in accordance with the procedure described in Sec. 2, we obtained almost equal SPM-induced phase shifts $\varphi_{SPM}^1 = 11.268$ (rad) and $\varphi_{SPM}^2 = 11.264$ (rad) with two-fold difference in pulse energies ($E_p^1 = 0.4$ nJ, $E_p^2 = 0.8$ nJ) and peak powers ($P_{peak}^1 = 50$ W, $P_{peak}^2 = 99$ W), which unambiguously proved an existence of optimized $\varphi_{SPM}^{max}$ associated with chirp value $C_{lin}$. It is worth to stress, that for longer fiber segment overall SC quality in terms of Strehl ratio is clearly increased ($S_1 = 0.5$, $S_2 = 0.43$), while other SC parameters including spectrum compression ratio ($K_S^1 = 14.2$, $K_S^2 = 12.8$), energy confinement ratio ($\eta_1 = 0.73$, $\eta_2 = 0.69$), and TBP ($TBP_1 = 0.84$, $TBP_2 = 0.93$) turn out to be improved as well. This result can be interpreted in such a way that longer fiber segment is preferable over higher input peak power to reach better SC quality, which is, however valid only for moderate peak powers from the middle range in accordance with Fig. 11a. Likewise, tighter beam focusing results in stronger aberration appearance.

Linear dependence of SCR on pulse stretching ratio $K_P$ depicted in Fig. 5a allows us to suggest linear relationship between optimized $\varphi_{SPM}^{max}$ and SCR as well. This assumption is clearly confirmed by high quality linear interpolation of $\varphi_{SPM}^{max}(K_S)$ dependence plotted on Fig. 13b with corresponding slope of $d\varphi_{SPM}^{max}/dK_S = 1.08 \pm 0.05$ and small offset value (≈1.9), which makes possible to claim approximate equality of optimized $\varphi_{SPM}^{max}$ and SCR (valid with greater accuracy for $K_S >> 1$): $\varphi_{SPM}^{max} = L_f \cdot \gamma \cdot P_{peak} \approx K_S$ (***). This criterion can be considered as a necessary guideline for SC optimization procedure.

Figure 14 shows maximum spectrum compression ratio evolution (red circles) with negative chirp growth, calculated for the input peak power of $P_{peak} = 100$ W and a fixed pulse spectrum width of 11 nm ($\tau_{min} = 0.33$ ps). For comparison, experimental data (blue squares) are plotted as well. Within negative chirp variation from $C_{lin} = -20$ to $-160$ (and corresponding pulse-width tuning from 6.7 ps to 53.3 ps) almost linear monotonous dependence of $K_S$ on $C_{lin}$ is observed, which is confirmed by high quality linear approximation with a slope of $|dK_S^{theory}/dC_{lin}| = 0.339 \pm 0.005$, being ≈1.5-times less than experimentally obtained value $|dK_S^{exp}/dC_{lin}| = 0.528 \pm 0.026$. As stated above, we attribute this divergence to the different contributions from the nonlinear part of the pulse chirp to the SPM-induced spectrum compression for highly-chirped Gaussian and real pulses resulting in different partial compensation for a nonlinear phase modulation imposed by SPM. Indeed, as evidently seen in Fig. 14, for SCR less than ∼10, corresponding to negative chirp values up to $C_{lin} \approx -25$, experimental and theoretical SCR values are well-consistent.

It should be noted that spectrum compression process at the peak power of $P_{peak} = 100$ W occurs similarly to that shown in Fig. 8 and 9 for negative chirp values up to $C_{lin} = -100$. For larger chirp values (ranged from $C_{lin} = -130$ to $C_{lin} = -160$), modulation instability-induced distortions of the pulse envelope and spectrum originate, like those shown in Fig. 10.

From numerical analysis, it follows that for negatively chirped picosecond Gaussian pulses propagating in the low-loss dispersion-shifted telecom fiber near its zero dispersion wavelength, SPM-induced spectrum compression with $K_S = 50 \div 60$ and energy confinement exceeding 50% can be achieved at moderate peak powers of ~100 W and negative chirp values in the range from $C_{lin} = -160$ to $C_{lin} = -130$. Furthermore, for negative chirp values up to $C_{lin} \approx -100$ and nonlinear phase shift of $\varphi_{SPM} \approx 80$ rad, the process of negative chirp compensation in the vicinity of maximum compression point occurs under symmetrical modulation structure development only in the pulse spectrum, whereas pulse envelope disturbance is strictly negligible. However, its growth limits the optimal fiber length at which it is possible to obtain a compressed spectrum with sufficiently high pulse energy. Within further increase in the chirp magnitude ($|C_{lin}| > 100$), the spectrum compression process is strongly affected by combined action of SPM and fiber dispersion resulting in severe distortions of the spectral and temporal pulse characteristics.

## 6. Conclusions

In conclusion, we studied both experimentally and numerically self-phase modulation-induced spectrum compression dynamics of negatively chirped picosecond Gaussian pulses in the low-loss dispersion-shifted telecom fiber near its zero dispersion wavelength. Via SMF-LS fiber length and pulse peak power adjustment, we observed nearly linear monotonous growth of spectrum compression ratio from $K_S = 4.5$ to 49.2 within a linear chirp variation from $C_{lin} = -5.9$ to $-91.9$ (and corresponding pulse-width tuning between 2.5 ps and 38.3 ps). In contrast to spectrum compression ratio, energy confinement ratio goes down from $\eta = 77\%$ to 50% while TBP value grows from 0.76 to 1.06, the latter exhibiting saturation behavior, which leads to saturation trend of the Strehl ratio evolution with the negative chirp growth, and thus, favors SCR rising without stagnation of brightness increase.

According to numerical simulations, fiber dispersion was found to be responsible for limiting both SCR growth and spectrum compression quality expressed in terms of time-bandwidth product value and energy confinement ratio at larger chirp values ($|C_{lin}| > 100$), owing to self-phase modulation-governed complex propagation dynamics of highly-chirped Gaussian pulses in the vicinity of zero dispersion wavelength of the fiber. Moreover, in order to obtain an SCR higher than 50, experimentally realized at $|C_{lin}| \sim 100$, fibers with a lower positive dispersion in the spectral band occupied by a chirped pulse are required.

Through fiber length and pulse energy optimization, we achieved record 49.2-fold spectrum compression of 38.3-ps, 2.08 nJ negatively-chirped Gaussian pulses with compressed spectrum FWHM of 0.23 nm and ≈50% energy confinement ratio at 1560 nm wavelength, corresponding to ≈13.3-fold spectral brightness magnification.

We believe that results obtained can be promising for ultra-short pulse laser systems development with enhanced spectral brightness.

## Acknowledgment

Authors are grateful to L.V. Kotov and M.E. Likhachev from FORC RAS for the help in high-power MOCPA erbium fiber source development. Authors also thank S.G. Sazonkin from BMSTU, B.L. Davydov from IRE RAS and T.A. Kochergina from FORC RAS for technical support.

## References

[1] M. E. Fermann, A. Galvanauskas, and G. Sucha, *Ultrafast Lasers: Technology and Applications*. New York, NY, USA: Marcel Dekker, 2001.
[2] S. A. Diddams, "The evolving optical frequency comb [Invited]," *J. Opt. Soc. Am. B.*, vol. 27, no. 11, pp. B51–B62, 2010.
[3] M. E. Fermann and I. Hartl, "Ultrafast fiber laser technology," *IEEE J. Sel. Topics Quantum Electron.*, vol. 15, no. 1, pp. 191–206, Jan. 2009.

[4] J. Kim and Y. Song, "Ultralow-noise mode-locked fiber lasers and frequency combs: Principles, status, and applications," *Adv. Opt. Photon.*, vol. 8, pp. 465–540, 2016.
[5] http://avesta.ru/products/lasers/femtosekundnie-volokonnie-laseri/
[6] http://www.menlosystems.de/
[7] Th. Udem, R. Holzwarth, and T. W. Hänsch, "Optical frequency metrology," *Nature*, vol. 416, pp. 233–237, 2002.
[8] Florian Adler *et al.*, "Phase-locked two-branch erbium-doped fiber laser system for long-term precision measurements of optical frequencies," *Opt. Exp.*, vol. 12, no. 24, pp. 5872–5880, 2004.
[9] R. A. McCracken, J. M. Charsley, and D. T. Reid, "A decade of astrocombs: Recent advances in frequency combs for astronomy [Invited]," *Opt. Exp.*, vol. 25, no. 13, pp. 15058–15078, 2017.
[10] Y. Nomura *et al.*, "Supercontinuum generation for ultrahigh-resolution optical coherence tomography at wavelength of 0.8$\mu$m using carbon nanotube fiber laser and similariton amplifier," *Appl. Phys. Exp.*, vol. 7, 2014, Art. no. 122703.
[11] T. Nishitani, T. Konishi, and K. Itoh, "Resolution improvement of all-optical analog-to-digital conversion employing self-frequency shift and self-phase-modulation-induced spectral compression," *IEEE J. Sel. Topics Quantum Electron.*, vol. 14, no. 3, pp. 724–732, May-Jun. 2008.
[12] N. Nishizawa and K. Takahashi, "Time-domain near-infrared spectroscopy using a wavelength-tunable narrow-linewidth source by spectral compression of ultrashort soliton pulses," *Opt. Lett.*, vol. 36, no. 19, pp. 3780–3782, 2011.
[13] E. R. Andresen, V. Birkedal, J. Thogersen, and S. R. Keiding, "Tunable light source for coherent anti-Stockes Raman scattering microspectroscopy based on the soliton self-frequency shift," *Opt. Lett.*, vol. 31, no. 9, pp. 1328–1330, 2006.
[14] J. Lavoie, J. M. Donohue, L. G. Wright, A. Fedrizzi, and K. J. Resch, "Spectral compression of single photons," *Nature Photon.*, vol. 7, pp. 363–366, 2013.
[15] E. R. Andresen, J. M. Dudley, D. Oron, C. Finot, and H. Rigneault, "Transform-limited spectral compression by self-phase modulation of amplitude-shaped pulses with negative chirp," *Opt. Lett.*, vol. 36, no. 5, pp. 707–709, 2011.
[16] M. Rusu and O. G. Okhotnikov, "All-fiber picosecond laser source based on nonlinear spectral compression," *Appl. Phys. Lett.*, vol. 89, pp. 1–3, 2006, Art. no. 091118.
[17] J. Fatome, B. Kibler, E. R. Andresen, H. Rigneault, and C. Finot, "All-fiber spectral compression of picosecond pulses at telecommunication wavelength enhanced by amplitude shaping," *Appl. Opt.*, vol. 51, no. 19, pp. 4547–4553, 2012.
[18] M. Oberthaler and R. A. Höpfel, "Special narrowing of ultrashort laser pulses by self-phase modulation in optical fibers," *Appl. Phys. Lett.*, vol. 63, no. 8, pp. 1017–1019, 1993.
[19] E. R. Andresen, J. Thøgersen, and S. R. Keiding, "Spectral compression of femtosecond pulses in photonic crystal fibers," *Opt. Lett.*, vol. 30, no. 15, pp. 2025–2027, 2005.
[20] J. Limpert, T. Gabler, A. Liem, H. Zellmer, and A. Tunnerman, "SPM-induced spectral compression of picosecond pulses in a single-mode Yb-doped fiber amplifier," *Appl. Phys. (B)*, vol. 74, pp. 191–195, 2002.
[21] J. Limpert *et al.*, "High-power picosecond fiber amplifier based on nonlinear spectral compression," *Opt. Lett.*, vol. 30, no. 7, pp. 714–716, 2005.
[22] L. Kh. Mouradian, F. Louradour, V. Messager, A. Barthélémy, and C. Froehly, "Spectro-temporal Imaging of Femtosecond Events," *IEEE J. Quantum Electron.*, vol. 36, no. 7, pp. 795–801, Jul. 2000.
[23] M. A. Kalashyan, K. A. Palandzhyan, G. L Esayan, L. Kh Muradyan, "Generation of transform-limited rectangular pulses in a spectral compressor," *Quantum Electron.*, vol. 40, no. 10, pp. 868–872, 2010.
[24] S. T. Cundiff *et al.*, "Propagation of highly chirped pulses in fiber-optic communications systems," *J. Lightw. Technol.*, vol. 17, no. 5, pp. 811–815, May 1999.
[25] X. Liu and Y. Cui, "Flexible pulse-controlled fiber laser," *Scientific Rep.*, vol. 5, p. 5, 2015, Art. no. 9399.
[26] B. R. Washburn, J. A. Buck, and S. E. Ralph, "Transform-limited spectral compression due to self-phase modulation in fibers," *Opt. Lett.*, vol. 25, no. 7, pp. 445–447, 2000.
[27] S Boscolo, L Kh Mouradian, and C Finot, "Enhanced nonlinear spectral compression in fiber by external sinusoidal phase Modulation," *J. Opt.*, vol. 18, p. 7, 2016, Art. no. 105504.
[28] C. Finot and S. Boscolo, "Design rules for nonlinear spectral compression in optical fibers," *J. Opt. Soc. America B*, vol. 33, no. 4, pp. 760–767, 2016.
[29] Y. Chen *et al.*, "All-fiber low-pedestal spectral compression in a novel architecture based on an SMF cascading an HNLF-NOLM," *IEEE Photon. J.*, vol. 6, no. 5, p. 8, Oct. 2014, Art. no. 6100408.
[30] C. Bao, X. Xiao, and C. Yang, "Spectral compression of a dispersion-managed mode-locked Tm: Fiber laser at 1.9 $\mu$m," *IEEE Photon. Technol. Lett.*, vol. 28, no. 4, pp. 497–500, Feb. 2016.
[31] A. A. Krylov *et al.*, "1.56 $\mu$m sub-microjoule femtosecond pulse delivery through low-loss microstructured revolver hollow-core fiber," *Laser Phys. Lett.*, vol. 14, no. 3, p. 7, 2017, Art. no. 035104.
[32] S. O. Leonov, V. S. Voropaev, and A. A. Krylov, "Pump- and temperature-induced repetition frequency response study in hybrid mode-locked erbium fiber laser with distributed polarizer," *Appl. Phys. B (Lasers Opt.)*, vol. 125, no. 39, p. 11, 2019.
[33] L. V. Kotov *et al.*, "Submicrojoule femtosecond erbium-doped fibre laser for the generation of dispersive waves at submicron wavelengths," *Quantum Electron.*, vol. 44, no. 5, pp. 458–464, 2014.
[34] A. E. Levchenko, A. S. Kurkov, and S. L. Semenov, "Measurement of dispersion in optical fibres with a microstructure cladding," *Quantum Electron.*, vol. 35, no. 9, pp. 835–838, 2005.
[35] J. Dudley and R. Taylor, *Supercontinuum Generation in Optical Fibers*, Cambridge, U.K.: Cambridge, Univ. Press, 2010.
[36] S. Wang, W. Chen, P. Qin, Y. Song, M. Hu, B. Liu, "Spectral and temporal breathing self-similar evolution in a fiber amplifier for low-noise transform-limited pulse generation," *Opt. Lett.*, vol. 41, no. 22, pp. 5286–5289, 2016.